Off-Target ^{18}F-AV-1451 Binding in the Basal Ganglia Correlates with Age-Related Iron Accumulation

Jae Yong Choi[1,2], Hanna Cho[3], Sung Jun Ahn[4], Jae Hoon Lee[1], Young Hoon Ryu[1], Myung Sik Lee[3], and Chul Hyoung Lyoo[3]

[1]*Department of Nuclear Medicine, Gangnam Severance Hospital, Yonsei University College of Medicine, Seoul, Republic of Korea;*
[2]*Division of Rhode Island-Convergence Research, Korea Institute Radiological and Medical Sciences, Seoul, Republic of Korea;*
[3]*Department of Neurology, Gangnam Severance Hospital, Yonsei University College of Medicine, Seoul, Republic of Korea; and*
[4]*Department of Radiology, Gangnam Severance Hospital, Yonsei University College of Medicine, Seoul, Republic of Korea*

See an invited perspective on this article on page 115.

Off-target binding in the basal ganglia is commonly observed in the ^{18}F-AV-1451 PET studies of the elderly. We sought to investigate the relationship between this phenomenon in the basal ganglia and iron accumulation using iron-sensitive R_2* MRI. **Methods:** Fifty-nine healthy controls and 61 patients with Alzheimer disease and mild cognitive impairment underwent ^{18}F-AV-1451 PET and R_2* MRI studies. A correlation analysis was performed for age, ^{18}F-AV-1451 binding, and R_2* values. **Results:** There was an age-related increase in both ^{18}F-AV-1451 binding in the basal ganglia and R_2* values in the putamen in both the controls and the Alzheimer disease/mild cognitive impairment patients. ^{18}F-AV-1451 binding in the basal ganglia increased with R_2* values. **Conclusion:** Off-target ^{18}F-AV-1451 binding in the basal ganglia is associated with the age-related increases in iron accumulation. Postmortem studies are required to further investigate the nature of this association.

Key Words: ^{18}F-AV-1451; PET; iron; aging; basal ganglia

J Nucl Med 2018; 59:117–120
DOI: 10.2967/jnumed.117.195248

The most widely investigated tau-selective radiotracer, ^{18}F-AV-1451, has high affinity to paired helical filaments of tau protein in Alzheimer disease (AD) and low or intermediate affinity to straight filaments of tau in various non-AD tauopathies (*1*). However, ^{18}F-AV-1451 also binds to structures with high neuromelanin or melanin content and the choroid plexus, which is considered to be off-target binding (*1,2*). Additionally, increased ^{18}F-AV-1451 binding in the basal ganglia is commonly observed even in the healthy elderly (*1,3,4*), and appears to be age-related (*4*).

A previous autoradiography study showed sparse patterns of nonspecific ^{18}F-AV-1451 binding in the basal ganglia in the absence of noticeable tau pathology (*3*). Other studies showed weak ^{18}F-AV-1451 binding in the lesions with acute or subacute hemorrhage (*1*) and a topographic similarity between ^{18}F-AV-1451 binding in the basal ganglia and areas stained by iron-sensitive Prussian blue, hinting at an association between the ^{18}F-AV-1451 and iron accumulation (*2*). However, this association has not been confirmed, and the nature of this off-target ^{18}F-AV-1451 binding in the basal ganglia remains unclear.

In this study, we investigated the relationship between aging, ^{18}F-AV-1451 binding, and iron accumulation in the basal ganglia using iron-sensitive R_2* MRI. We also explored the relationship between ^{18}F-AV-1451 binding and R_2* values in the basal ganglia of healthy controls and a composite group of patients with amnestic mild cognitive impairment (MCI) and AD.

MATERIALS AND METHODS

Subjects

We selected subjects from a consecutive cross-sectional cohort recruited for a tau PET study. For the inclusion in the tau PET study cohort, a criteria of probable AD proposed by the National Institute of Neurologic and Communicative Disorders and Stroke and the Alzheimer Disease and Related Disorders Association (*5*) and the Petersen's criteria (*6*) were used for clinical diagnosis of AD and MCI, respectively. All AD and MCI patients initially presented with memory disturbance, and no patient presented with atypical clinical features for variant AD (posterior cortical atrophy, logopenic aphasia, or frontal-variant AD). We also included healthy controls with no neurologic abnormality, no memory complaint, and normal cognition on the Korean version of the Mini-Mental State Examination score. No subject showed greater than mild-to-moderate white matter changes on fluid-attenuated inversion recovery MR images. In this study cohort, 151 subjects underwent quantitative MRI with R_2* sequence. According to amyloid positivity as determined by the consensus of 2 nuclear medicine specialists using visual assessment of ^{18}F-florbetaben PET images (*7*), 59 amyloid-negative controls, 29 amyloid-positive MCI, and 32 amyloid-positive AD patients were selected for this study. The AD and MCI patients were combined to create a composite AD/MCI group for simplicity.

This study was approved by the Institutional Review Board of Gangnam Severance Hospital, and written informed consent was obtained from all participants.

Acquisition of PET and MR Images

We synthesized ^{18}F-AV-1451 by the nucleophilic substitution of ^{18}F on the N-Boc nitro precursor. The radiochemical purity was 98%, and specific activity was greater than 250 GBq/μmol at the end of synthesis.

Received Apr. 25, 2017; revision accepted Jul. 5, 2017.
For correspondence or reprints contact either of the following:
Chul Hyoung Lyoo, Department of Neurology, Gangnam Severance Hospital, Yonsei University College of Medicine, 20 Eonjuro 63-gil, Gangnam-gu, Seoul, South Korea.
E-mail: lyoochel@yuhs.ac
Young Hoon Ryu, Department of Nuclear Medicine, Gangnam Severance Hospital, Yonsei University College of Medicine, 20 Eonjuro 63-gil, Gangnam-gu, Seoul, South Korea.
E-mail: ryuyh@yuhs.ac
Published online Aug. 3, 2017.

PET images were acquired from 80 to 100 min after the intravenous injection of 280.3 ± 36.5 MBq of ^{18}F-AV-1451 using a Biograph mCT PET/CT scanner (Siemens Medical Solutions). Before the PET scan, a head holder was applied to minimize motion during the scan, and brain CT images were acquired for attenuation correction. After correcting for attenuation and scatter, 3-dimensional PET images were reconstructed in a 256 × 256 × 223 matrix with 1.591 × 1.591 × 1 mm voxel size using the ordered-subsets expectation maximization algorithm. Likewise, amyloid PET images were acquired from 90 to 110 min after the injection of 302.7 ± 39.9 MBq of ^{18}F-florbetaben.

R_2* MR images were acquired on a 3.0-T MR scanner (Discovery MR750; GE Healthcare) with a multiecho fast spoiled gradient echo sequence (repetition time, 65 ms; echo time, 12, with a regular interval from 1.9 to 27.4 ms; flip angle, 20°; slice thickness, 2.5 mm). Using in-house software implemented in MATLAB 7.1 (The MathWorks), we estimated R_2* values of each voxel by regression of log signals of the 12 multiecho volumes. For the structural imaging, T1-weighted MR images were acquired with 3-dimensional spoiled gradient-recalled sequences (repetition time, 8.28 ms; echo time, 1.6–11.0 ms; flip angle, 20°; matrix, 512 × 512; voxel spacing, 0.43 × 0.43 × 1 mm).

Image Processing Steps

We used FreeSurfer 5.3 (Massachusetts General Hospital, Harvard Medical School; http://surfer.nmr.mgh.harvard.edu) for creating subject-specific volume-of-interest mask images. T1-weighted MR images were corrected for inhomogeneity and segmented into gray and white matter. Subcortical structures were segmented using a probabilistic registration method (*8*), and subject-specific composite volume-of-interest mask images for 4 subcortical regions (caudate, putamen, globus pallidus, and cerebellar cortex) were created. PET images were coregistered to the MR images, and then SUV ratio (SUVR) images were created using the binding value of the cerebellar cortex. Regional SUVRs were measured by overlaying the subject-specific composite volume-of-interest mask images on the PET images. Likewise, R_2* images were coregistered to the MR images, and regional R_2* values were measured with the same volume-of-interest mask images.

We used statistical parametric mapping 8 (Wellcome Department of Cognitive Neurology) and in-house software implemented in MATLAB for the voxel-based analysis. Coregistered SUVR images of ^{18}F-AV-1451 PET and R_2* images were spatially normalized to in-house diffeomorphic anatomic registration using an exponentiated lie algebra template by applying a flow-field normalizing the segments for gray and white matter (*9*). Before voxel-based analysis, spatially normalized SUVR and R_2* images were smoothed with 8 mm in full width at half maximum.

Statistical Analysis

We used SPSS 23 (IBM Corp.) for the statistical analysis. The independent *t* test and χ^2 tests were used for the comparison of continuous and categoric variables in the demographic data, respectively. For the comparison of regional subcortical binding values of ^{18}F-AV-1451 PET and R_2* values, we used an analysis of covariance model with age as a covariate. Pearson correlation analysis was used for the investigation of the correlation analysis among age, ^{18}F-AV-1451 binding values, and R_2* values.

A simple correlation model was used for the voxel-based correlation analysis between age and either ^{18}F-AV-1451 binding or R_2* values. For the voxel-based correlation between the ^{18}F-AV-1451 PET and R_2* MR images, we used Pearson correlation analysis with an in-house MATLAB program. When a template brain mask was used, voxels with a false-discovery rate of less than 0.05 were considered significant.

RESULTS

The demographic characteristics of the 2 subject groups are summarized in Supplemental Table 1 (supplemental materials are available at http://jnm.snmjournals.org). AD/MCI patients were generally older and had a higher frequency of the apolipoprotein E ε4 genotype, and worse global cognition as determined by Mini-Mental State Examination and Clinical Dementia Rating sum-of-boxes scores, compared with the controls. There were no differences in sex or years of education between the 2 groups.

Mean putaminal ^{18}F-AV-1451 SUVRs for the AD/MCI patients were slightly greater than those of the controls after adjusting for age ($P = 0.023$). However, there were no differences in ^{18}F-AV-1451 SUVRs for the caudate and globus pallidus or for any subcortical R_2* values between the controls and AD/MCI patients (Table 1).

In the control group, ^{18}F-AV-1451 SUVRs for all 3 regions correlated highly with age ($P < 0.001$). Similarly, SUVRs for the

TABLE 1
Regional ^{18}F-AV-1451 SUVR and R_2* Values

Groups/ regions	^{18}F-AV-1451			R_2*			R_2* vs. ^{18}F-AV-1451	
		Age vs. ^{18}F-AV-1451			Age vs. R_2*			
	Mean SUVR ± SD	*r*	*P*	Mean R_2* (s^{-1}) ± SD	*r*	*P*	*r*	*P*
HC								
Caudate	1.21 ± 0.19	0.463	<0.001	22.6 ± 2.0	0.218	0.096	0.453	<0.001
Putamen	1.54 ± 0.27	0.585	<0.001	28.6 ± 3.6	0.433	<0.001	0.549	<0.001
Pallidum	1.75 ± 0.29	0.445	<0.001	39.6 ± 5.1	0.039	0.772	0.324	0.012
AD/MCI								
Caudate	1.32 ± 0.17	0.163	0.210	22.6 ± 2.3	0.085	0.513	0.255	0.048*
Putamen	1.77 ± 0.26†	0.373	0.003	30.6 ± 5.3	0.221	0.087	0.445	<0.001
Pallidum	1.91 ± 0.25	0.391	0.002	38.0 ± 5.2	0.001	0.996	0.227	0.079

*$P < 0.05$ for comparisons between HC (healthy control) and AD/MCI groups after adjusting for age.

†Regions failed to survive region-wise correction for multiple comparisons.

Data are presented as mean ± SD for regional SUVR and R_2* values, and Pearson correlation coefficients (*r*) and their *P* values are also presented.

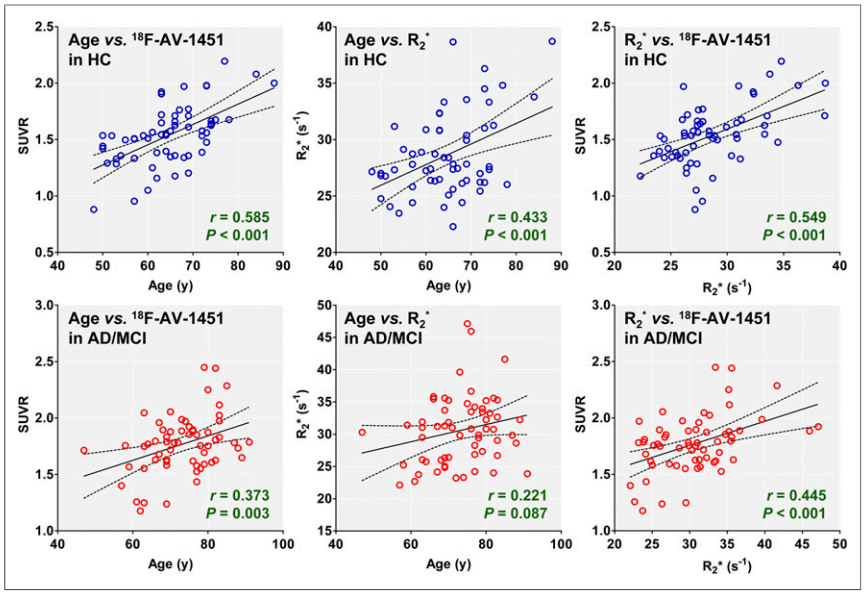

FIGURE 1. Scatterplot showing correlation among age, ^{18}F-AV-1451 SUVRs, and R_2* values of putamen. With exception of weak trend for correlation between age and R_2* values in AD/MCI group, ^{18}F-AV-1451 SUVR and R_2* values increased with advancing age and ^{18}F-AV-1451 SUVRs correlated with R_2* values in both HC and AD/MCI groups. HC = healthy control.

putamen and globus pallidus correlated with age in AD/MCI patients. Putaminal R_2* values correlated with age in the controls ($P < 0.001$), but no region showed correlation in AD/MCI patients. There was a small increasing trend for R_2* values with age ($P = 0.087$). Regional ^{18}F-AV-1451 SUVRs correlated with R_2* values for the caudate, putamen, and globus pallidus in the controls and for the caudate ($P = 0.048$, failed to survive multiple comparisons) and putamen in AD/MCI patients (Table 1; Fig. 1).

In voxel-based analysis, ^{18}F-AV-1451 binding increased with age in all basal ganglia regions, most prominently in the putamen of the controls. In contrast, the correlation was observed only in the smaller anterior putamen in the AD/MCI patients. Similarly, putaminal R_2* signal correlated with age in controls, but only the small anterior putamen showed a correlation in AD/MCI patients. ^{18}F-AV-1451 binding increased with R_2* signal in the caudate and putamen in the controls, whereas AD/MCI patients also showed a correlation between 2 imaging parameters in the anterior putamen (Fig. 2; Supplemental Fig. 1).

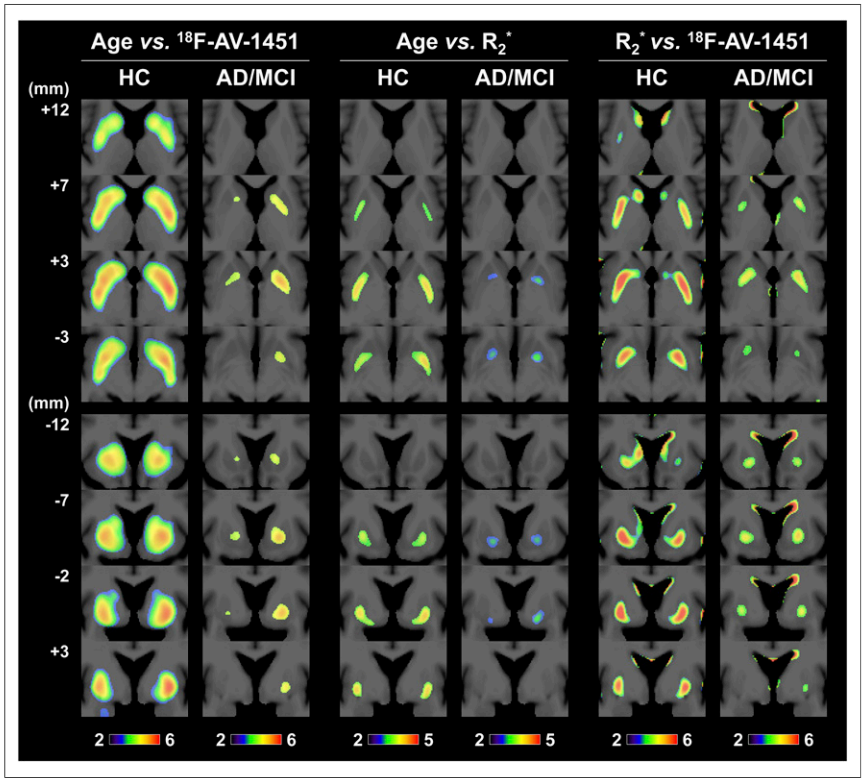

FIGURE 2. Voxel-based analysis results for correlation among age, ^{18}F-AV-1451 SUVRs, and R_2* values Coordinates for each slice are presented as numbers on left side of figure (distance from anterior commissure: from ventral to dorsal for axial images and from rostral to caudal for coronal images). Color scale bars represent -$\log_{10}$ *P* values. HC = healthy control.

DISCUSSION

Brain iron concentration is highest in the globus pallidus, followed by the red nucleus, substantia nigra, putamen, dentate nucleus, caudate nucleus, and thalamus (*10*). Although increases in pallidal iron plateau after the first 3 decades of life and pallidal iron is less affected by age thereafter, iron levels in the putamen and caudate steadily increase after middle age (*10,11*). Antemortem iron-sensitive MR studies have shown regional vulnerability and age-related changes in iron accumulation as was observed in our study (*12*). Moreover, the regional gradient for ^{18}F-AV-1451 binding within the basal ganglia was similar to that of the R_2* values in this study, whereas ^{18}F-AV-1451 binding values for each region within the basal ganglia correlated with both age and R_2* values in controls. Although weaker than in the controls, the age-related correlation between the 2 parameters was also observed in the putamen in the AD/MCI group. These suggest that there should be a direct or indirect relationship between the ^{18}F-AV-1451 and iron.

Unlike transferrin (a major iron-transporting protein), which shows a uniform distribution pattern throughout the gray matter, ferritin (a major iron-storage protein) generally correlates with tissue iron levels and increases with age (*13,14*). Neuromelanin also plays a role in the sequestration of brain iron and exists in the basal ganglia, premotor cortex and cerebellum, as well as substantia nigra (*15*). Although neuromelanin pigment concentration also increases with age in all of these regions, there is no notable

difference in concentrations between regions other than the substantia nigra (*15*). Considering regional distribution and age-related changes, iron or ferritin is a possible target of ^{18}F-AV-1451 off-target binding. However, alternative scenarios should also be considered due to no ^{18}F-AV-1451 binding to the lesions in superficial siderosis (*1*) and lack of regional correspondence between ^{18}F-AV-1451 binding and iron-sensitive staining in neurodegeneration with brain iron accumulation (*2*).

CONCLUSION

Off-target ^{18}F-AV-1451 binding in the basal ganglia is associated with age-related iron accumulation. Postmortem studies are required to further investigate the nature of this association and mechanism of off-target binding.

DISCLOSURE

This study was financially supported by the "Mirae Medical" Faculty Research Assistance Program of Yonsei University College of Medicine (grant no. 6-2016-0162), a National Research Foundation of Korea (NRF) grant funded by the Korean government (MSIP) (no. 2015R1C1A2A01054507), Basic Science Research Program through the National Research Foundation of Korea (NRF) funded by the Ministry of Science, ICT & Future Planning (2017R1A2B2006694), and a Nuclear R&D Program of the National Research Foundation of Korea (no. NRF-2016M2A2A7024357). No other potential conflict of interest relevant to this article was reported.

ACKNOWLEDGMENTS

We express our special appreciation to Tae Ho Song and Won Taek Lee (PET technologists) who managed all PET scans with enthusiasm.

REFERENCES

1. Marquié M, Normandin MD, Vanderburg CR, et al. Validating novel tau positron emission tomography tracer [F-18]-AV-1451 (T807) on postmortem brain tissue. *Ann Neurol.* 2015;78:787–800.
2. Lowe VJ, Curran G, Fang P, et al. An autoradiographic evaluation of AV-1451 tau PET in dementia. *Acta Neuropathol Commun.* 2016;4:58.
3. Passamonti L, Vazquez Rodriguez P, Hong YT, et al. ^{18}F-AV-1451 positron emission tomography in Alzheimer's disease and progressive supranuclear palsy. *Brain.* 2017;140:781–791.
4. Smith R, Schain M, Nilsson C, et al. Increased basal ganglia binding of 18 F-AV-1451 in patients with progressive supranuclear palsy. *Mov Disord.* 2017;32:108–114.
5. McKhann G, Drachman D, Folstein M, Katzman R, Price D, Stadlan EM. Clinical diagnosis of Alzheimer's disease: report of the NINCDS-ADRDA Work Group under the auspices of Department of Health and Human Services Task Force on Alzheimer's Disease. *Neurology.* 1984;34:939–944.
6. Petersen RC, Smith GE, Waring SC, Ivnik RJ, Tangalos EG, Kokmen E. Mild cognitive impairment: clinical characterization and outcome. *Arch Neurol.* 1999;56:303–308.
7. Sabri O, Sabbagh MN, Seibyl J, et al. Florbetaben PET imaging to detect amyloid beta plaques in Alzheimer's disease: phase 3 study. *Alzheimers Dement.* 2015;11:964–974.
8. Fischl B, Salat DH, Busa E, et al. Whole brain segmentation: automated labeling of neuroanatomical structures in the human brain. *Neuron.* 2002;33:341–355.
9. Ashburner J. A fast diffeomorphic image registration algorithm. *Neuroimage.* 2007;38:95–113.
10. Hallgren B, Sourander P. The effect of age on the non-haemin iron in the human brain. *J Neurochem.* 1958;3:41–51.
11. Ramos P, Santos A, Pinto NR, Mendes R, Magalhaes T, Almeida A. Iron levels in the human brain: a post-mortem study of anatomical region differences and age-related changes. *J Trace Elem Med Biol.* 2014;28:13–17.
12. Daugherty A, Raz N. Age-related differences in iron content of subcortical nuclei observed in vivo: a meta-analysis. *Neuroimage.* 2013;70:113–121.
13. Ward RJ, Zucca FA, Duyn JH, Crichton RR, Zecca L. The role of iron in brain ageing and neurodegenerative disorders. *Lancet Neurol.* 2014;13:1045–1060.
14. Haacke EM, Cheng NY, House MJ, et al. Imaging iron stores in the brain using magnetic resonance imaging. *Magn Reson Imaging.* 2005;23:1–25.
15. Zecca L, Bellei C, Costi P, et al. New melanic pigments in the human brain that accumulate in aging and block environmental toxic metals. *Proc Natl Acad Sci USA.* 2008;105:17567–17572.